Interaction of T-10 Plasma with Impurity Pellets and Supersonic Gas Jet

V.Yu. Sergeev 1), V.M. Timokhin 1), V.G. Skokov 1), B.V. Kuteev 2), S.V. Krylov 2), L.N. Khimchenko 2), and T-10 team 2)

1) State Polytechnical University, St. Petersburg, Russia
2) Nuclear Fusion Institute, Russian Research Center "Kurchatov Institute", Moscow, Russia

e-mail contact of main author: sergeev@phtf.stu.neva.ru

Abstract. The 0.3 mm carbon pellet diameter threshold of an appearance of the enhanced pellet ablation rate at the fixed T-10 plasma parameters is experimentally observed. Ablation rate profiles of smaller pellets can be reasonable described by Neutral Gas Shielding (NGS) Model predictions. Radial positions of the enhanced ablation zones was closed to the fast electron temperature perturbations during the pellet ablation. The pre-cooling front velocity may exceed the pellet velocity up to one order of magnitude. Predictions of the improved NGS model by taking into account the reconnection events can reasonably describe radial profiles of the measured ablation rate for large carbon pellets. Cylindrical pellets with $(1.6–2.2)\cdot10^{19}$ lithium atoms were injected in 4 subsequent shots aiming the improvement of the plasma purity. Unfortunately, no essential effect was indicated. The He gas jet injection was arranged by means the fast valve with a Laval nozzle. Good enough "fuelling" efficiency of the injected matter was detected.

Introduction

The high temperature plasma fuelling by hydrogen pellets, plasma diagnostics and discharge control (wall conditioning, disruption mitigation) by means of impurity pellets are widely used in tokamaks and stellarators [1,2,3]. One of the crucial parameters of the pellet-plasma interaction problem is a pellet penetration depth into the plasma. It depends on the pellet shielding effect by the pellet clouds [4], suprathermal particle fluxes in plasma [5], and MHD processes in plasma including those initiated by a pellet [6]. Another important problem in pellet-plasma interaction is a fast transport of the pellet the pellet ablated material ablated.

The toroidal drifts of plasmoids generated by the pellet ablation [7] or MHD processes [6,8] could be responsible for this redistribution of the pellet material. Understandings of both mechanisms are very important for a further development of plasma diagnostics, fuelling and plasma control by means of pellet injection. First section of the report is devoted to the carbon pellet injection experiments where MHD events occurring during ablation and an attendant transport of the pellet material are investigated.

The high temperature plasma discharge control is one of important tasks in the program of the controlled fusion achievement [3]. The first wall lithium (Li) conditioning in TFTR, T-11M, FTU, CDX-U tokamaks was found as a factor of a significant decrease of the carbon recycling that leaded to low impurity content in the plasma column [9-11]. On the other hand, it had not been confirmed in either Heliotron E [12] or Alcator C MOD [13] Li pellet experiments. Supersonic jets of hydrogen and impurity gases are being applied for plasma fueling [14] and disruption mitigation [15] correspondingly. The recent theoretical calculations predict a good penetration capability for gas jets in the plasma column [16]. Second and third sections are devoted to description of the first T-10 experiments on Li-conditioning and helium jet injection.

1. Impurity pellets ablation features

1.1. Experimental setup

The spherical carbon pellets with the varied $d = 0.2 \div 0.62$ mm diameters ($1.9\times10^{17} \div 5.1\times10^{18}$ atom content were accelerated up to 400 m/s by the gas dynamic impurity pellet injector [17] towards the plasma center in top-bottom direction [6]. Pellets with more than 0.5 mm in diameter penetrated beyond the plasma center the 0.62 mm size pellets went through the Ohmically heated plasma column with the following parameters: $\langle n_e \rangle \approx 2\times10^{13}$ cm^{-3}, T_e = 1,2 keV, I_{pl} = 270 kA, B_t = 2,4 T, a_L = 30 cm, q_L = 3. The pellet ablation was measured by the CCD camera which registered the pellet track, and by meant of the wide view angle photodetector with a 1 μs temporal resolution. Both detectors were equipped by the interference filter corresponding to the CII 723 nm line which intensity I_{CII} is proportional to the pellet ablation rate $\dot{N}(t)$ [18].

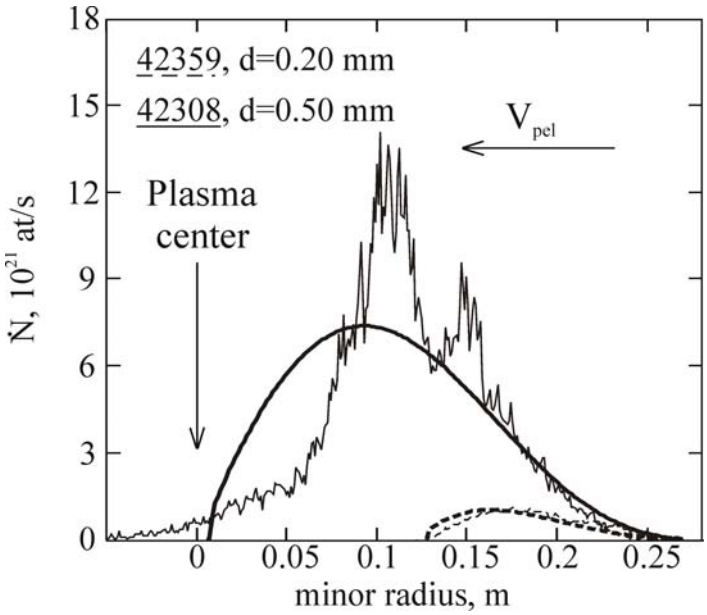

Fig. 1. Experimentally measured (fine lines) and simulated according to NGSM (thick lines) ablation rate profiles for pellets of different diameters. NGSM simulation results were obtained without taking reconnections in account. Solid lines:#42359 V_{pel} =393 m/s, dashed lines# 42308 – 348 m/s. The experimentally measured plasma density and temperature profile used for simulations in the paper were approximated as $3{,}4 \cdot 10^{13} \cdot (1-(\frac{r}{a})^2)^{1,2}$ *cm^{-3} and* $1200 \cdot (1-(\frac{r}{a})^{2,3})^2$ *eV correspondingly.*

1.2. Experimental results

In experiments were observed an appearance of the enhanced pellet ablation zones which had the clearly pronounced threshold versus the injected pellet diameter (see Fig. 1). The ablation rate values for pellets with d < 0.3 mm were fairly well corresponded to the Neutral Gas Shielding Model (NGSM) [4] predictions and a probability of the enhanced pellet ablation appearance did not exceed 30%. In the cases of fairy large pellets (d > 0.3 mm) this probability becomes 100%.

A fast temporal behavior of the electron temperature profiles during pellet ablation into plasma were measured by the ECE super-heterodyne detector [19] and shown in Fig. 2. One can see a threshold character of the propagation of cooling fronts. The V_{cool} cooling front velocity were evaluated using the relationship shown in Fig. 2. It is seen that the (t_6–t_5), (t_2–t_1)

are significantly lower than (t_5–t_4), (t_4–t_3), (t_3–t_2) ones. This fact indicates the fast cooling fronts forming in vicinity of r_1 and r_6.

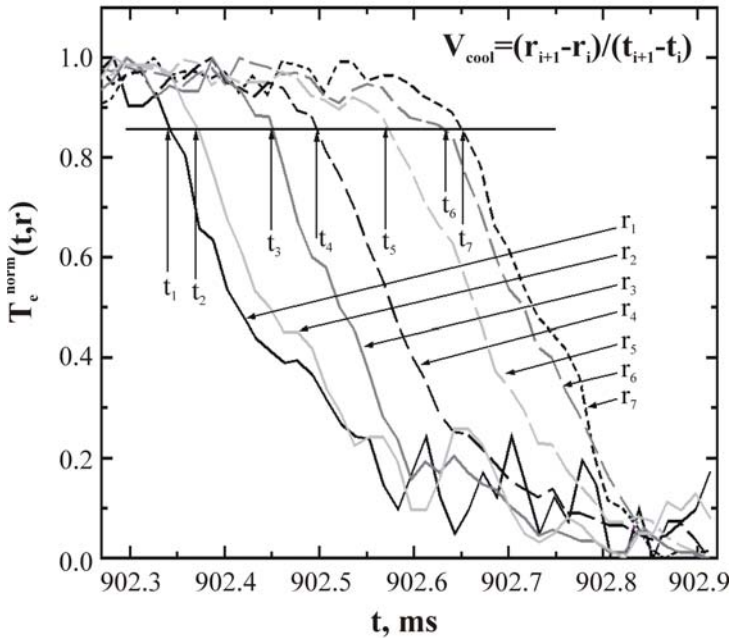

Fig. 2. Normalized Te signals illustrating the appearance of the cooling fronts with velocities V_{cool} that are significantly higher than V_{pel}. The distance between the observation points r_{i+1}-r_i = 1.8 cm. Time moments t_i were determined by a 15% decrease of the T_e at r_i.

Measured $\gamma = V_{cool}/V_{pel}$ ratios and the wide view angle photodetector signals I_{CII} for pellets of different diameters are shown in Fig. 3. For pellets with $d < 0.3$ mm these velocities are close, so that γ is of about 1 (Fig. 3a). But for bigger pellets the drastic growth of γ in several narrow zones can be seen (Fig. 3b,c). These zones appeared close to the enhanced pellet ablation zones. The maximal γ ratio value > 10 was observed in the central plasma region in vicinity of saw-tooth mixing radius (Fig. 3c).

In cases of small pellets no precooling effect were observed, while with larger pellets those occurred with a probability of about 20%. It is necessary to mark that the ablated pellet material propagation with velocities significantly higher that the pellet velocity was also observed by the AXUVD diode arrays [20] earlier.

1.3. Simulations and discussion

The data obtained point out that the pellet ablation and ablated material transport mechanisms during the pellet penetration into the plasma might depend on MHD processes localized close to rational magnetic surfaces. For explanation of the observed enhanced ablation rate zones and a generation of heat and particles fast fronts the model NGSM was improved taking into account the MHD reconnection driven by the pellet as follows.

The pellet cools plasma and adds impurity in it, so the effective charge Z_{eff} grows at the position of the ablated pellet. It results in a growth of the resistivity η and electric field. Then, it might cause a formation of X-points for helical magnetic flux reconnections in vicinity of rational magnetic surfaces [21]. The estimations show that this effect could be very strong: typical resistive time $\tau_R = r^2/\eta$ can decrease in 10^3-10^4 times because the electron

temperature close to the pellet is lower than 10 eV [1]. So the tearing mode islands with width w of order of several centimeters can grow during time intervals which are much less than 100 μs values being typical for the $T_e \cong 1$ keV and $Z_{eff} \cong 2$ T-10 Ohmically heated plasmas. Besides, the Kadomtsev's reconnection time can reach the microsecond range during the pellet injection as well. Small microsecond characteristic times of the tearing mode development and Kadomtsev's reconnection due to pellet ablation are significantly lees than pellet ablation time. It allows us to propose the following algorithm of the pellet ablation rate simulation taking in account the reconnection events.

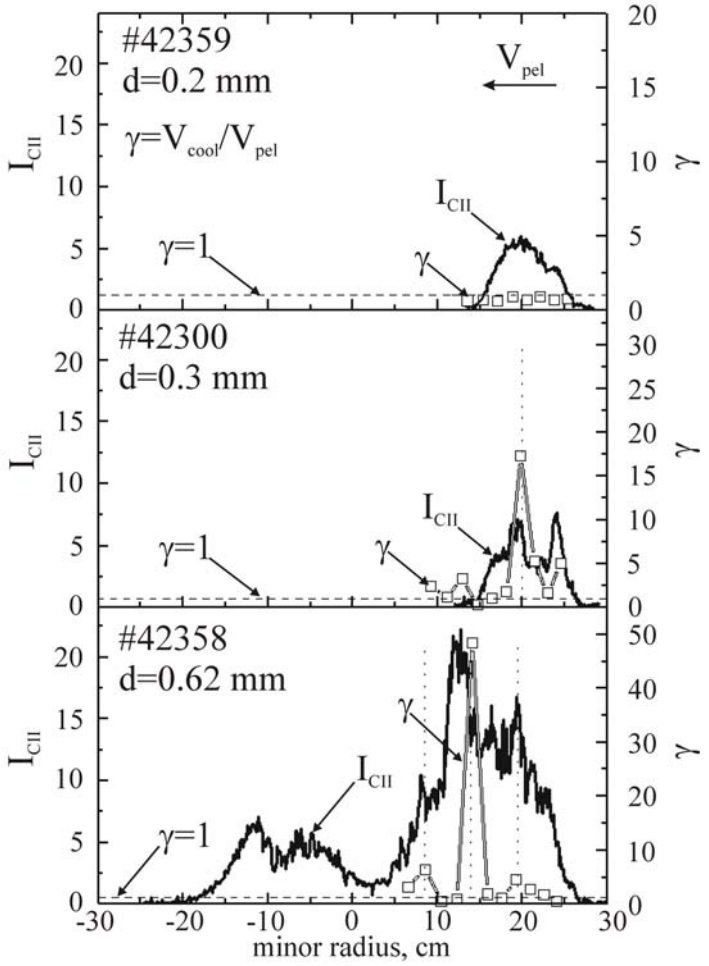

Fig. 3. Comparison of the ablation rate and the cooling front propagation velocity. Pellet diameters are shown in the figure notes. Negative minor radius values are corresponding to the region of the pellet propagation below the midplane.

The NGSM [4] is used for calculations of the ablation rate $\dot{N}(t)$ which depends on the electron density and temperature at the current pellet position r in the plasma and also on the current pellet diameter. Starting from the plasma boundary $r = a_L$ right up to the point where the enhanced ablation rate starts, the ablation rate profile $\dot{N}(r)$ is calculated using the unperturbed density $n_e(r)$ and temperature $T_e(r)$ values. We assume that tearing mode islands, which w = 3-4 cm width can be estimated from the observed distance between the spikes on the ablation rate profile, are forming instantly (forming time ~1 μs corresponds to pellet displacement ≤ 0.4 mm) as pellet reaches the rational magnetic surface with q = 2, 3/2, 4/3 and 5/4. The plasma mixing in reconnection zones forms new n_e and T_e profiles in front of the

pellet at the *w/2* distance. The ablation rate $\dot{N}(r)$ after the reconnection event is simulated using these new profiles. In our calculations the instant ionization of ablated carbon up to Z = 6 is assumed. When pellet reaches the q = 1 magnetic surface we use the Kadomtsev's reconnection model and modified n_e and T_e profiles [22]. Beyond the plasma center n_e and T_e profiles are calculated taking in account the pellet material ablated prior the magnetic axis. In this region, reconnection effects were not taken into account for simplicity and the radiative losses in energy balance equation were taken in account with the 5 kev per carbon atom [18].

Fig. 4 illustrates the simulation results according to the improved NGSM. In this figure the experimentally measured ablation rate (fine solid line) is being compared with calculating according to NGSM predictions done without (thick solid line) and with those where the reconnection phenomena was taken account (fine dashed line). One can note that the model with reconnection reasonably describes the experimentally observed ablation rate behavior. Moreover, the modeled ablation rate behavior inside the q = 1 surface with Kadomtsev's reconnection event is reasonably agree with experimental one. Even beyond the plasma center the experimental and calculated ablation rate profiles demonstrate similar behavior.

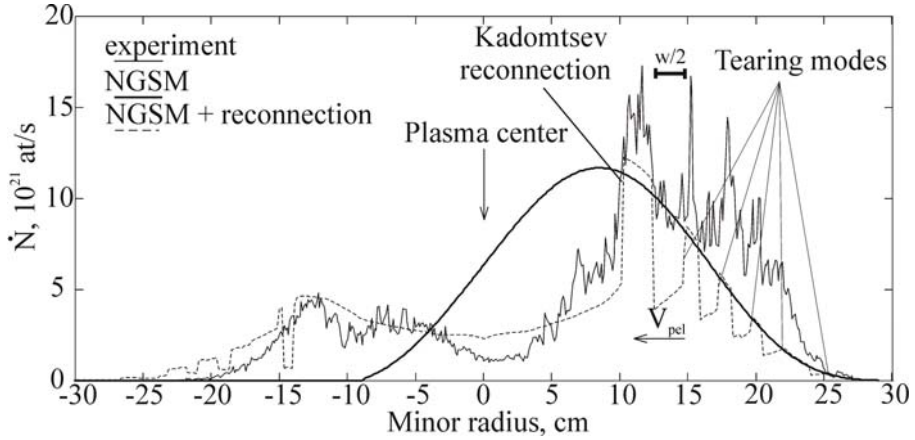

Fig. 4. Pellet ablation simulation results taking in account reconnections during the pellet penetration into plasma. Pellet velocity V_{pel} = 371 m/s, pellet diameter d = 0.62 mm.

1.4. Conclusions

The $d_{thr} \cong$ 0.3 mm carbon pellet diameter threshold of an appearance of the enhanced pellet ablation rate at the fixed T-10 plasma parameters is experimentally observed. Ablation rate profiles of smaller pellets can be reasonable described by NGSM predictions. Radial positions of the enhanced ablation zones close to the fast electron temperature perturbations during the pellet ablation. The pre-cooling front velocity may exceed the pellet velocity up to one order of magnitude.

The possible explanation of the observed phenomena is based on the assumption that the pellet produces plural x-points at q = 2, 3/2, …; and single x-point at q = 1 magnetic surface and excites reconnections due to the plasma conductivity decrease in x-points. It occurs due to both electron temperature drop and the effective charge Z_{eff} rise in a vicinity of the ablated pellet that causes significant growth of the tearing mode increment on rational surfaces and the essential decrease of to the resistive reconnection time q = 1. Predictions of the improved NGS model by taking into account the reconnection events can reasonably describe radial profiles of the measured ablation rate for large carbon pellets.

The observed MHD processes ensure the deeper penetration of the pellet itself as well as ablated material into the plasma. It could increase the pellet fuelling efficiency in the reactor.

The pellet initiated reconnections and the consequent convective transport are depended on the safety factor profile, so they can appear during the pellet injection from any direction. In that case the pellet injection from “high field side” and “low field side” directions should demonstrate close results of pellet ablation and deposition into the plasma.

2. Discharge conditioning experiments

In the Li experiments, cylindrical pellets of 0.75-0.78 mm in diameter and 0.9±0.1 mm in length which corresponds to (1.6–2.2)x10^{19} lithium atoms content were injected. The pellet size was limited by the pellet injector barrel size. Before injection Li pellets were coated with (LiN_3) lithium nitride shell of 10 mkm thickness. This procedure was used for avoiding the undesirable effect of lithium sticking with injector material and allowed to accelerate Li pellets up to 650 m/s velocities in the direction of plasma core with fairly good probability.. Details of the injector experimental setup are presented in [23]. Injections were carried out in OH+ECRH heated plasma with following main parameters: $<n_e>$ = 3x10^{13} cm^{-3}, I_p= 270 kA, B_t = 2.4 T, P_{ECRH} = 800 kW. Li pellets penetrated up to 10 cm of the a_L = 30 cm T-10 minor radius and deposited most part of lithium around of a half of a_L.

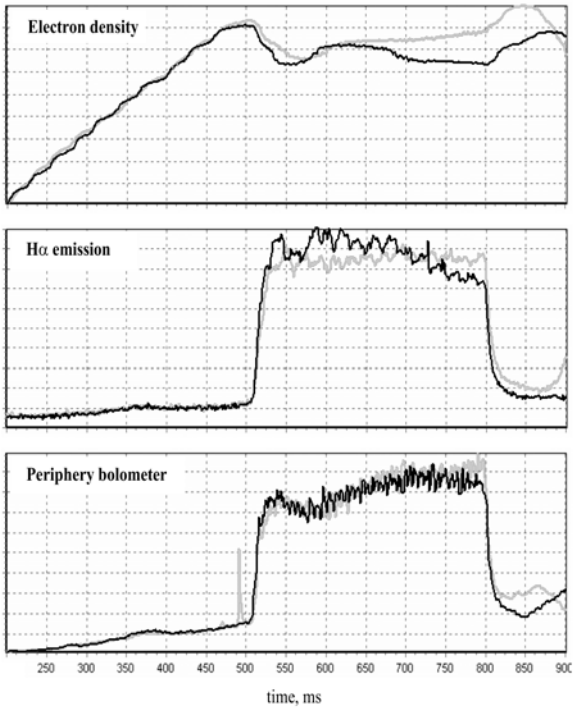

Fig. 5. Evolution of main plasma parameters in the reference shots before (#42312 light curve) and after (#42319 dark curve) a sequence of Li pellet injection. All data are in arbitrary units.

The estimation of a lithium amount for the one monolayer coating of the T-10 first wall surface gives a number of 2.5x10^{20} Li atoms which 10 times higher then the pellet content. On the other hand a direct contact with a high-temperature plasma column has the limiter surface only. It is enough ~10^{18} Li atoms to coat the T-10 limiter surface. In the case of direct Li deposition to the limiter, especially with effect of cumulative (from shot to shot) Li accumulation presence, one can expect of desirable effects of the Li discharge conditioning.

In the experiment the Li pellet injected at 600 ms of discharge, 100 ms latter than the switching on time of the ECRH gyrotron power. The hydrogen puff valve that controls the

plasma density in the discharge was stopped at injection moment to clarify the subsequent changes of the recycling coefficient. Besides, a special regime of the discharge shutdown without the toroidal magnetic field cessation has been used to exclude the lithium washout during the shutdown duration. A sequence of 4 shots with Li pellet injection was realized (##42313, 42315, 42316, and 42317). Two reference shots without Li injection before (#42312) and after (#42319) the sequence has been analyzed in order to observe the conditioning effects. In the shots #42314 and #42318 were no plasma due to technical problems.
The temporal behavior of signals obtained by the central microwave interferometer channel, H_α detector and one of peripheral bolometer channels (30 cm of minor radius) are presented in Fig. 5. It is seen that obvious effects of the discharge cleaning is absent. A qualitative composition of peripheral impurities had no noticeable disturbance after Li injection sequence because the peripheral bolometer signal demonstrate the similar behavior with these measured in reference shots. An analysis of main impurities lines radiation (CIII, OII) leads to the same conclusion because no significant differences in the impurities line radiation power before and after a sequence with Li injection are observed. The possible reason of absence of the Li pellet conditioning effect is insufficient total amount of injected Li.

One can be seen from Fig. 5 that the electron density decreased after the Li injection sequence in spite of its increasing in the shot before injection. It occurred since 600 ms after the hydrogen gas puff valve was closed. It implies a decrease of the hydrogen recycling due to the Li pellet injection.

3. Supersonic He jet injection

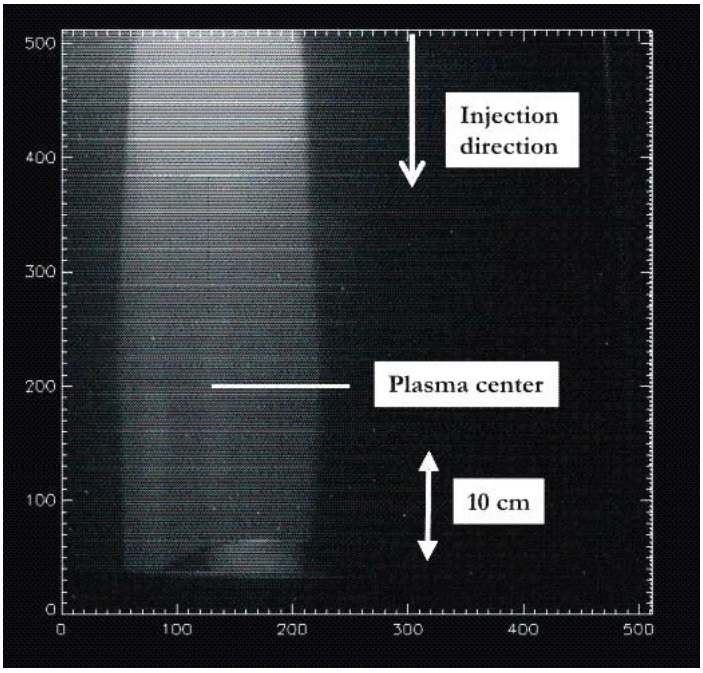

Fig. 6. He supersonic jet penetration in T-10 plasma.

The gas injection was arranged using the supersonic jet source developed and mounted at T-10 recently. The jet source consists the fast electromagnetic fast valve and the Laval nozzle. The nozzle has 3 mm in length and the 0.3 mm throat size. The valve opening duration time is about 2 ms that allows to inject (1-20)x10^{19} He atoms depended on the (5-100 bar) pressure before the valve. A forming of the compact helium jet with ~1.5 km/s velocity was evaluated. So that He was intruded into the plasma by injecting the jet from top to bottom toward the

axis of the plasma column. Injections were carried out in the Ohmically heated plasma with $<n_e>$ = 3x10^{13} cm^{-3} , I_p = 270 kA, a_L = 30 cm and a varied number of the injected helium atoms. It was shown that injection of more than 3x10^{19} atoms caused the discharge minor disruption. In a case of moderate pressure, the He amount calculated from the nozzle flow dynamics (1.2x10^{19} atoms) and measured (1.6x10^{19} atoms) in the test bed experiments fairly good agrees with He deposited 1.5x10^{19} atoms which was evaluated using the electron density increase after injection. It reveals a good enough "fueling" efficiency of the He jet injected.

The jet emission in plasma was observed through continuum light filter using the CCD camera (see Fig. 6). One can roughly estimate the ~12 cm He jet penetration radius depth that corresponds to 0.6·a_L. Further activity presumes studies of jet penetration depth versus jet velocity, sort of injected gas, plasma density and a comparison with theoretical predictions [16]. A discharge shutdown experiment with the massive Ar gas jet injection is foreseen as well.

Acknowledgements

This work was partially supported by RFBR grants ## 05-02-17269, 06-02-17333 and grant of RF President to young scientist supporting # MK-7792.2006.2.

References

[1] S.L. Milora, W.A. Houlberg, L.L. Lengyel, V. Mertens, Nucl. Fusion **35**, 657 **(**1995).
[2] B.V. Kuteev, Techn. Phys. **69**, 63 (1999).
[3] Technical Basis for the ITER Final Design Report (2001).
[4] B.V. Kuteev, V.Yu. Sergeev, L.D. Tsendin, Sov. J. Plasma Phys. **10**, 675 (1984).
[5] V.M. Timokhin, B.V. Kuteev, V.Yu. Sergeev et al., Techn. Phys. Letters **30**, 298 (2004).
[6] B. Kuteev, L. Khimchenko, S. Krylov et al., 32nd EPS Conf. on Plasma Phys., 2005, ECA Vol. **29C**, O-1.002.
[7] V.A. Rozhansky, I. Veselova, S. Voskoboynikov, Plasma Phys. Control. Fus. **37**, 399 (1995).
[8] H.R. Strauss, W. Park, E. Belova et al., Nucl. Fusion **39**, 2069 (1999).
[9] Mirnov S V et al., Plasma Phys. Control. Fusion **48** (2006) 821–837.
[10] Mansfield D.K. et al., J. Phys. Plasmas **3** (1996) 1892.
[11] Majeski R. et al., Nucl. Fusion **45** (2005) 519–523.
[12] Sergeev V.Yu. et al., Plasma Phys. Control. Fusion **40** (1998) 1785.
[13] J. Rice, private communication.
[14] Bucalossi J. et al., EPS Conf. on Plasma Phys. Tarragona, Vol.**29C**, O-4.005 (2005).
[15] Hollmann E.M. et.al, Nuclear Fusion **45** (2005) 1046.
[16] Rozhansky V. et.al, Nucl. Fusion **46** (2006) 367-382.
[17] S.M. Egorov, et al., Nuclear Fusion vol. 32, No. 11 (1992), pp. 2025-2028
[18] L. Ledl, R. Burhenn, L. Lengyel, et al., Nuclear Fusion, **44** (2004), p. 600-608.
[19] V.I. Poznyak, A.V. Bludov, Yu.K. Ermishkina et al., in: Proc. of 10th Russian Conf. on Plasma Diagn. (Troitsk, Russia, June 2003), B6, p. 10-11.
[20] L. Khimchenko, B. Kuteev, S. Krylov et al., 33rd EPS Conf. on Plasma Phys. Roma, 19 – 23 June 2006, P4-090.
[21] E. Priest and T. Forbs, Magnetic Reconnection, MHD Theory and Applications, Cambridge, University Press, 2000.
[22] B.B. Kadomtsev, Sov. J. Plasma Phys. **1**, 389 (1975).
[23] BelopolskyV.A. et al., Europhys. Conf. Abs., St. Petersburg, Vol.**27A**, P-3.117 (2003).